Analysis of Moving Loads on the Surface of a Cylindrical Bore using Neural Network

Mansour Nikkhah-Bahrami*, Arman Hajati, Omid Rohani
Mechanical Engineering Department
University of Tehran, Tehran, Iran
e-mail: mbahrami@ut.ac.ir

Abstract

This paper considers a line load applied along a transverse circle that travels in the axial direction along the interior of a circular bore in an infinite elastic, homogenous and isotropic medium. The stresses and displacements in the medium, expected to reach a steady-state value, are obtained analytically using Fourier series and Laplace transform. The solution has an integral form; therefore, a feedforward backpropagation neural network is designed and trained using the response evaluated numerically in a finite set of random points to approximate stresses and displacement components in the medium.

1 Introduction

1.1 General Remarks

There has been considerable interest in the interaction of stress waves with cylindrical cavities. Most of the recent study has resulted from the requirement for underground protective structures. The object of this paper is to obtain stress and displacement for a line load applied along a transverse circle that travels in the axial direction along the interior of a circular bore in an infinite elastic, homogenous and isotropic medium. A possible application here would be the analysis of tunnels subjected to the air induced ground shock in the super seismic region of an explosion. The line load has an arbitrary distribution in the angular coordinate along the circumference of the circle and moves with a constant velocity, which is greater than the propagation velocities of the dilatational and equivoluminal waves in the elastic medium; therefore, the speed is superseismic with respect to these waves.

From a general consideration of wave propagation, it is clear that there can be no stress or displacements ahead of the leading front; this fact permits us to use Laplace transform. The stresses and displacements in the medium are expected to reach a steady-state value; i.e., to appear as independent of time in a moving coordinates system. To obtain the solution, the applied line load and expression for the stresses and displacements components can be expanded into a Fourier series in terms of the angular coordinate. Laplace transform of stresses and displacement components can be derived for each term of the Fourier series in a closed form. Having applied inverse Laplace transform, the components can be found analytically as a function of the radial distance from the cavity axis and the longitudinal distance behind the wave in integral form. Generally, the integral form can not be simplified to simple forms. For that reason, numerical integration methods should be used to evaluate the infinite integral for which a considerable amount of computations is required [6]. Because of the significant amount of the numerical computation needed, the solutions were expressed only on the boundary of the bore in the previous works. Nowadays, intelligent methods such as neural networks can be used as powerful tools for calculating the response. Therefore, soft computing can be exploited to estimate the response in every points of the medium in the vicinity of the front load.

1.2 Problem Description

The object of this work is to obtain stresses in an elastic medium in the vicinity of a cylindrical cavity which is engulfed by a plane stress wave of dilatational travelling parallel to the axis of the cylinder, as shown in Figure 1. The load has an arbitrary distribution $P(\theta)$ along the circumference of the circle and moves with a velocity$V > c_p > c_s$; therefore, the speed is super seismic with respect to both the dilatational and shear waves in the medium. Consequently, the disturbances which were initiated far behind the front on the boundary of the cavity cannot reach the vicinity of the wave front for some time after the incident wave passes.

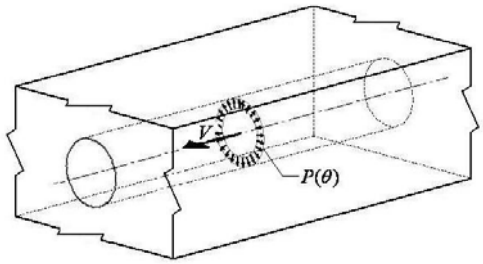

Figure 1 : Moving line load

Moreover, because of the super seismic nature of the problem, it should be expected that two mach cones will be formed in the medium, as shown in Figure 2. These cones should open toward the rear of the front. Furthermore, there can be no stresses or displacements ahead of the leading front. Accordingly, because of the boundary condition we can use Laplace transform to solve the problem by transforming the partial differential equations into ordinary differential equations.

If a coordinate system is assumed to move along the cylinder with the wave front, it is seen that the state of stress at points close behind the wave front depend only on relative position of them with respect to the front. Thus, in the vicinity of the wave front, provided that the end of the cavity is far away, the problem may be treated as a steady-state case. In other words, in the moving coordinate system, the state of stress and displacement is independent of time.

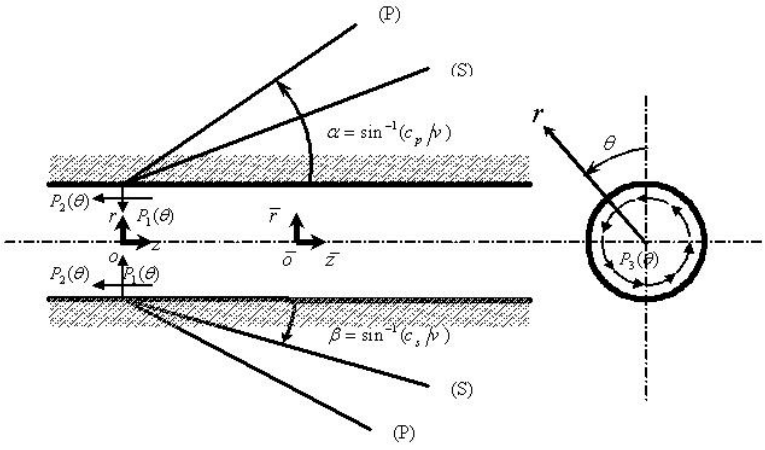

Figure 2 : Geometry of the problem and the coordinate systems

Method of Solution

The method of solution is somehow similar to that used in [1], [2], [3]. Because of the steady-state nature in the moving coordinates, all the variables are assumed to be time-invariant and the wave equation is transformed into a 3 dimensional partial differential equations. To solve these PDEs analytically, Fourier series and Laplace transform are used to transform them into ordinary differential equations.
The stress fields and also the displacement fields are expanded in Fourier series in terms of the angle, θ, around the bore. The Fourier series of the moving pressure is determined at any points in medium. The stress fields are expressed in terms of potential functions that satisfy the equations of motion. Explicit expressions for the transformed stresses and displacements in the medium are briefly given for all cases, $n \geq 0$. A complete analytical and numerical analysis is done for axisymmetric case, $(n = 0)$. Stress and displacement components in terms of potential functions are written in Laplace domain and the wave equations is transformed into modified Bessel equations. Using the boundary conditions, the solution is found for each term of stress and displacement components in Laplace domain. Therefore, by applying inverse Laplace transform, the solution is obtained in integral form for each term. Numerical integration of infinite complex integrals is carried on using adaptive Lobatto integration method to find the solution for a set of points in the vicinity of wave front. The numerical integration is really time-consuming; therefore, a multilayer feedforward backpropagation neural network is employed to estimate the solution in the medium. The network is trained using the numerical solution for a set of points and successfully tested and verified in estimating the solution. Finally, all of the components of stress and displacement are evaluated by means of simulating the network.

2 General Formulation

Consider a plane dilatational wave travelling along the interior of the cavity with a velocity of V. Let $\left(r,\theta,\bar{z}=a\bar{\zeta}\right)$ be cylindrical coordinates whose origin lies on the axis of the cavity. Now suppose that the origin of a new coordinates system is allowed to move along the $\bar{z}$ axis with the wave front. Therefore the transformation from $\left(r,\theta,\bar{z}\right)$ coordinate system to $\left(r,\theta,z\right)$ system is accomplished by the following relations:

$$r = r\,, \qquad \theta = \theta, \qquad \zeta = \frac{z}{a} = \frac{1}{a}(\bar{z} + vt) \tag{1}$$

The propagation velocities of dilatational and equivoluminal waves in the medium c_p, c_s are related to the medium density ρ and Lame constants λ, μ by

$$c_p = \sqrt{\frac{\lambda + 2\mu}{\rho}}\,, \qquad c_s = \sqrt{\frac{\mu}{\rho}} \tag{2}$$

We suppose Mach numbers M, M_s to be

$$M = \frac{V}{c_p} > 1\,, \qquad M_s = \frac{V}{c_s} > 1 \tag{3}$$

The equation of motion for a linearly elastic medium is

$$\mu\nabla^2\mathbf{u} + (\lambda + \mu)\nabla\nabla.\mathbf{u} = \rho\ddot{\mathbf{u}} \tag{4}$$

Where the displacement vector $\mathbf{u}$ in $\left(r,\theta,\bar{z}\right)$ coordinate system is

$$\mathbf{u}(r_1,\theta_1,z_1,t) = w(r_1,\theta_1,z_1,t)\mathbf{e_r} + v(r_1,\theta_1,z_1,t)\mathbf{e}_\theta + u(r_1,\theta_1,z_1,t)\mathbf{e_z} \tag{5}$$

The equation of motion, Eq.4, referred to the moving coordinate system $\left(r,\theta,z\right)$ becomes in the steady state form of

$$\mu\nabla^2\mathbf{u} + (\lambda + \mu)\nabla\nabla.\mathbf{u} = \rho\frac{v^2}{a^2}\frac{\partial^2\mathbf{u}}{\partial\zeta^2} \tag{6}$$

In which the displacement is

$$\mathbf{u}(r,\theta,z) = w(r,\theta,z)\mathbf{e}_r + v(r,\theta,z)\mathbf{e}_\theta + u(r,\theta,z)\mathbf{e}_z \tag{7}$$

The load has an arbitrary distribution $P(\theta)$ along the circumference of the circle. Three following cases of line loads are considered: normal to the surface, tangential to the surface in the direction of the axis of the bore, and tangential to the circle of load application, as shown in Figure 2.

2.1 Solution Expansion Using Fourier Series

The stresses on the boundary $r = a$ according to the moving coordinate system (r,θ,z), using Fourier series are

$$\sigma_{rr} = \frac{P_1}{a}(\theta)\delta(\zeta) = \sum_{n=0}^{\infty}\frac{P_{1,n}}{a}\delta(\zeta)\cos n\theta \tag{8}$$

$$\sigma_{rz} = \frac{P_2}{a}(\theta)\delta(\zeta) = \sum_{n=0}^{\infty}\frac{P_{2,n}}{a}\delta(\zeta)\cos n\theta \tag{9}$$

$$\sigma_{r\theta} = \frac{P_3}{a}(\theta)\delta(\zeta) = \sum_{n=0}^{\infty}\frac{P_{3,n}}{a}\delta(\zeta)\cos n\theta \tag{10}$$

Where the $\delta(\zeta)$ is the Dirac-delta function at $\zeta = 0$ .Also, the Fourier series of displacement components are

$$w(r,\theta,\zeta) = \sum_{n=0}^{\infty} w_n(r,\zeta)\cos n\theta \tag{11}$$

$$v(r,\theta,\zeta) = \sum_{n=1}^{\infty} v_n(r,\zeta)\sin n\theta \tag{12}$$

$$u(r,\theta,\zeta) = \sum_{n=0}^{\infty} u_n(r,\zeta)\cos n\theta \tag{13}$$

We introduce potential functions [2]

$$\varphi(r,\theta,\zeta) = \sum_{n=0}^{\infty}\varphi_n(r,\zeta)\cos n\theta \tag{14}$$

$$\psi(r,\theta,\zeta) = \sum_{n=0}^{\infty}\psi_n(r,\zeta)\cos n\theta \tag{15}$$

$$\chi(r,\theta,\zeta) = \sum_{n=1}^{\infty}\chi_n(r,\zeta)\sin n\theta \tag{16}$$

Where

$$w_n(r,\zeta) = \frac{\partial}{\partial r}\varphi_n - \frac{1}{a}\frac{\partial^2}{\partial r\partial\zeta}\psi_n + \frac{n}{r}\chi_n \tag{17}$$

$$v_n(r,\zeta) = -\frac{n}{r}\varphi_n + \frac{n}{ra}\frac{\partial}{\partial\zeta}\Psi_n - \frac{\partial}{\partial r}\chi_n \tag{18}$$

$$u_n(r,\zeta) = \frac{1}{a}\frac{\partial}{\partial\zeta}\varphi_n + \frac{\partial^2}{\partial r^2}\psi_n + \frac{1}{r}\frac{\partial}{\partial r}\psi_n - \frac{n^2}{r^2}\psi_n \tag{19}$$

Substituting Eqs.11 to 13 and 17 to 19 into Eq.7, it is found that the potential functions satisfy the modified wave equations

$$\nabla^2\varphi_n = \frac{M^2}{a^2}\frac{\partial^2}{\partial\zeta^2}\varphi_n \tag{20}$$

$$\nabla^2\psi_n = \frac{M_s^2}{a^2}\frac{\partial^2}{\partial\zeta^2}\psi_n \tag{21}$$

$$\nabla^2\chi_n = \frac{M_s^2}{a^2}\frac{\partial^2}{\partial\zeta^2}\chi_n \tag{22}$$

The stresses in the medium may be expressed in the terms of the potential functions by substituting Eqs.17 to 19 into the stress-strain relation:

$$\sigma = \lambda \nabla . \mathbf{u}[\mathbf{I}] + \mu[\nabla \mathbf{u} + \mathbf{u} \nabla] \tag{23}$$

Hence,

$$\sigma_{rr}(r,\theta,\zeta) = \sum_{n=0}^{\infty} \sigma_{rr,n}(r,\zeta)\cos n\theta$$

$$\sigma_{rr,n} = \left[\lambda \left(\frac{\partial^2}{\partial r^2}\varphi_n + \frac{1}{r}\frac{\partial}{\partial r}\varphi_n - \frac{n^2}{r^2}\varphi_n + \frac{1}{a^2}\frac{\partial^2}{\partial \zeta^2}\varphi_n \right) + 2\mu \left(\frac{\partial^2}{\partial r^2}\varphi_n - \frac{1}{a}\frac{\partial^3}{\partial r^2 \partial \zeta}\psi_n + \frac{n}{r}\frac{\partial}{\partial r}\chi_n - \frac{n}{r^2}\chi_n \right) \right] \tag{24}$$

$$\sigma_{\theta\theta}(r,\theta,\zeta) = \sum_{n=0}^{\infty} \sigma_{\theta\theta,n}(r,\zeta)\cos n\theta \tag{25}$$

$$\sigma_{\theta\theta,n} = \left[\lambda \left(\frac{\partial^2}{\partial r^2}\varphi_n + \frac{1}{r}\frac{\partial}{\partial r}\varphi_n - \frac{n^2}{r^2}\varphi_n + \frac{1}{a^2}\frac{\partial^2}{\partial \zeta^2}\varphi_n \right) + \frac{2\mu}{r} \left(\frac{\partial}{\partial r}\varphi_n - \frac{n^2}{r}\varphi_n + \frac{n^2}{ar}\frac{\partial}{\partial \zeta}\psi_n - \frac{1}{a}\frac{\partial^2}{\partial r \partial \zeta}\psi_n + \frac{n}{r}\chi_n - n\frac{\partial}{\partial r}\chi_n \right) \right]$$

$$\sigma_{zz}(r,\theta,\zeta) = \sum_{n=0}^{\infty} \sigma_{zz,n}(r,\zeta)\cos n\theta \tag{26}$$

$$\sigma_{zz,n} = \left[\lambda \left(\frac{\partial^2}{\partial r^2}\varphi_n + \frac{1}{r}\frac{\partial}{\partial r}\varphi_n - \frac{n^2}{r^2}\varphi_n + \frac{1}{a^2}\frac{\partial^2}{\partial \zeta^2}\varphi_n \right) + 2\mu \left(\frac{1}{a^2}\frac{\partial^2}{\partial \zeta^2}\varphi_n - \frac{n^2}{ar^2}\frac{\partial}{\partial \zeta}\psi_n + \frac{1}{ar}\frac{\partial^2}{\partial r \partial \zeta}\psi_n + \frac{1}{a}\frac{\partial^3}{\partial r^2 \partial \zeta}\psi_n \right) \right]$$

$$\sigma_{rz}(r,\theta,\zeta) = \sum_{n=0}^{\infty} \sigma_{rz,n}(r,\zeta)\cos n\theta \tag{27}$$

$$\sigma_{rz,n} = \mu \left(\frac{2}{a}\frac{\partial^2}{\partial r \partial \zeta}\varphi_n + \frac{\partial^3}{\partial r^3}\psi_n + \frac{1}{r}\frac{\partial^2}{\partial r^2}\psi_n - \frac{n^2+1}{r^2}\frac{\partial}{\partial r}\psi_n + \frac{2n^2}{r^3}\psi_n - \frac{1}{a^2}\frac{\partial^3}{\partial r \partial \zeta^2}\psi_n + \frac{n}{ar}\frac{\partial}{\partial \zeta}\chi_n \right)$$

$$\sigma_{r\theta}(r,\theta,\zeta) = \sum_{n=1}^{\infty} \sigma_{r\theta,n}(r,\zeta)\sin n\theta \tag{28}$$

$$\sigma_{r\theta,n} = \mu \left[\frac{2n}{r}\left(\frac{\varphi_n}{r} - \frac{\partial}{\partial r}\varphi_n \right) + \frac{2n}{ar}\frac{\partial^2}{\partial r \partial \zeta}\psi_n - \frac{2n}{ar^2}\frac{\partial}{\partial \zeta}\psi_n + \frac{1}{r}\frac{\partial}{\partial r}\chi_n - \frac{n^2}{r^2}\chi_n - \frac{\partial^2}{\partial r^2}\chi_n \right]$$

$$\sigma_{\theta z}(r,\theta,\zeta) = \sum_{n=1}^{\infty} \sigma_{\theta z,n}(r,\zeta)\sin n\theta \tag{29}$$

$$\sigma_{\theta z,n} = \mu \left[-\frac{2n}{ar}\frac{\partial}{\partial \zeta}\varphi_n + \frac{n}{r}\left(\frac{n^2}{r^2}\psi_n + \frac{1}{a^2}\frac{\partial^2}{\partial \zeta^2}\psi_n - \frac{1}{r}\frac{\partial}{\partial r}\psi_n - \frac{\partial^2}{\partial r^2}\psi_n \right) - \frac{1}{a}\frac{\partial^2}{\partial r \partial \zeta}\chi_n \right]$$

2.2 Axisymmetric Analytical Solution (n=0)

For the axisymmetric case n=0, the stress components $\sigma_{r\theta}, \sigma_{z\theta}$ and the displacement component v vanishes. Therefore, the boundary equations, Eqs.8 to 10, would be

$$\sigma_{rr}\big|_{r=a} = \frac{P_1}{a}\delta(\zeta) \tag{30}$$

$$\sigma_{rz}\big|_{r=a} = \frac{P_2}{a}\delta(\zeta) \tag{31}$$

After simplifying the Eqs.20 to 22 and applying Laplace transform with respect to ζ (s is the transform variable)

$$\frac{\partial^2 \Phi}{\partial r^2} + \frac{1}{r}\frac{\partial \Phi}{\partial r} - m^2 \left(\frac{s}{a} \right)^2 \Phi = 0 \tag{32}$$

$$\frac{\partial^2 \Psi}{\partial r^2} + \frac{1}{r}\frac{\partial \Psi}{\partial r} - m_s^2 \left(\frac{s}{a} \right)^2 \Psi = 0 \tag{33}$$

In which

$$m^2 = M^2 - 1 > 0\,, \qquad m_s{}^2 = M_s{}^2 - 1 > 0 \tag{34}$$

The solution of Eqs.32 and 33 is in the form of modified Bessel functions as

$$\Phi(r,s) = \alpha K_0\left(\frac{mrs}{a}\right) \tag{35}$$

$$\Psi(r,s) = \beta K_0\left(\frac{m_s rs}{a}\right) \tag{36}$$

Applying Laplace transform to Eqs.24 to 29 and 17 to 19 for $n = 0$ and substituting Eqs.35 to 36, the transform for the stress and displacement respectively become

$$\bar{\sigma}_{rr} = \left[\alpha\left\{\lambda M^2\left(\frac{s}{a}\right)^2 K_0\left(\frac{mrs}{a}\right) + 2\mu\left(\frac{s}{a}\right)\left[\left(M^2-1\right)\left(\frac{s}{a}\right)^2 K_0\left(\frac{mrs}{a}\right) + \frac{m}{r}K_1\left(\frac{mrs}{a}\right)\right]\right\} - \beta\left\{2\mu m_s\left(\frac{s}{a}\right)^2\left[m_s\left(\frac{s}{a}\right)K_0\left(\frac{m_s rs}{a}\right) + \frac{1}{r}K_1\left(\frac{m_s rs}{a}\right)\right]\right\}\right] \tag{37}$$

$$\bar{\sigma}_{\theta\theta} = \alpha\left[\lambda M^2\left(\frac{s}{a}\right)^2 K_0\left(\frac{mrs}{a}\right) - 2\mu\frac{ms}{ra}K_1\left(\frac{mrs}{a}\right)\right] + \beta\mu\left[\frac{2m_s}{r}\left(\frac{s}{a}\right)^2 K_1\left(\frac{m_s rs}{a}\right)\right] \tag{38}$$

$$\bar{\sigma}_{zz} = \alpha\left[\left(\lambda M^2 + 2\mu\right)\left(\frac{s}{a}\right)^2 K_0\left(\frac{mrs}{a}\right)\right] + \beta\mu\left[2m_s{}^2\left(\frac{s}{a}\right)^3 K_0\left(\frac{m_s rs}{a}\right)\right] \tag{39}$$

$$\bar{\sigma}_{rz} = -\alpha\mu\left[2m\left(\frac{s}{a}\right)^2 K_1\left(\frac{mrs}{a}\right)\right] - \beta\mu\left[m_s\left(m_s{}^2 - 1\right)\left(\frac{s}{a}\right)^3 K_1\left(\frac{m_s rs}{a}\right)\right] \tag{40}$$

$$W = -\alpha\frac{ms}{a}K_1\left(\frac{mrs}{a}\right) + \beta m_s\left(\frac{s}{a}\right)^2 K_1\left(\frac{m_s rs}{a}\right) \tag{41}$$

$$U = \alpha\frac{s}{a}K_0\left(\frac{mrs}{a}\right) + \beta m_s{}^2\left(\frac{s}{a}\right)^2 K_0\left(\frac{m_s rs}{a}\right) \tag{42}$$

In which

$$\alpha = \frac{a}{\mu m_s s^2 \Delta}(\alpha_1 P_1 + \alpha_2 P_2)\,, \qquad \beta = \frac{a^2}{\mu m_s s^2 \Delta}(\beta_1 P_1 + \beta_2 P_2)$$

$$\alpha_1 = -\left(3M^2 - 2\right)m_s s K_1(m_s s)\,, \qquad \alpha_2 = 2m_s\left(m_s s K_0(m_s s) + K_1(m_s s)\right)$$

$$\beta_1 = 2mK_1(ms)\,, \qquad \beta_2 = \left(3M^2 - 2\right)K_0(ms) + \frac{2m}{s}K_1(ms) \tag{43}$$

$$\Delta = -\left[(3M^2-2)^2 s K_0(ms)K_1(m_s s) + 4m m_s s K_1(ms)K_0(m_s s) + 6M^2 m K_1(ms)K_1(m_s s)\right]$$

3 Response Evaluation

Expressions for the inversion Laplace integrals of the stress and displacement components in the medium for the axisymmetric load line are considered in tow cases .In case 1, we assume $\sigma_{rr}\big|_{r=a} = \frac{P_1}{a}\delta(\zeta)$, $\sigma_{rz}\big|_{r=a} = 0$ and in case 2, we assume $\sigma_{rr}\big|_{r=a} = 0$, $\sigma_{rz}\big|_{r=a} = \frac{P_2}{a}\delta(\zeta)$. Because of the linear behavior of the equations, we apply superposition principal to have the effects of both cases 1 and 2.

3.1 Inverse Laplace Transform

In case 1, the inversion Laplace integrals are

$$\frac{a\sigma_{\theta\theta}(r,\zeta)}{P_1} = \frac{1}{2\pi i}\int_{\gamma-i\infty}^{\gamma+i\infty}\frac{\Gamma_{\theta\theta,1}(r,\zeta)}{\Delta(s)}e^{s\zeta}ds \tag{44}$$

$$\frac{a\sigma_{zz}(r,\zeta)}{P_1} = \frac{1}{2\pi i}\int_{\gamma-i\infty}^{\gamma+i\infty}\frac{\Gamma_{zz,1}(r,\zeta)}{\Delta(s)}e^{s\zeta}ds \tag{45}$$

$$\frac{\mu w(r,\zeta)}{P_1} = \frac{1}{2\pi i}\int_{\gamma-i\infty}^{\gamma+i\infty}\frac{\mu}{P_1}W(r,s)e^{s\zeta}ds \tag{46}$$

$$\frac{\mu u(r,\zeta)}{P_1} = \frac{1}{2\pi i}\int_{\gamma-i\infty}^{\gamma+i\infty}\frac{\mu}{P_1}U(r,s)e^{s\zeta}ds \tag{47}$$

And in case 2, the inversion Laplace integrals are

$$\frac{a\sigma_{\theta\theta}(r,\zeta)}{P_2} = \frac{1}{2\pi i}\int_{\gamma-i\infty}^{\gamma+i\infty}\frac{\Gamma_{\theta\theta,2}(r,\zeta)}{\Delta(s)}e^{s\zeta}ds \tag{48}$$

$$\frac{a\sigma_{zz}(r,\zeta)}{P_2} = \frac{1}{2\pi i}\int_{\gamma-i\infty}^{\gamma+i\infty}\frac{\Gamma_{zz,2}(r,\zeta)}{\Delta(s)}e^{s\zeta}ds \tag{49}$$

$$\frac{\mu w(r,\zeta)}{P_2} = \frac{1}{2\pi i}\int_{\gamma-i\infty}^{\gamma+i\infty}\frac{\mu}{P_2}W(r,s)e^{s\zeta}ds \tag{50}$$

$$\frac{\mu u(r,\zeta)}{P_2} = \frac{1}{2\pi i}\int_{\gamma-i\infty}^{\gamma+i\infty}\frac{\mu}{P_2}U(r,s)e^{s\zeta}ds \tag{51}$$

The integration path is shown in Figure 3. In computing Integrals of Eqs.44, 45, 48 and 49 one may observe that when $s\to\infty$ the integrant limit is not zero and so the integral is undetermined. To solve this problem we use the modified Bessel functions series [13]

$$K_\eta(s) \approx \sqrt{\frac{\pi}{2s}}e^{-s}\left\{1+\frac{\kappa-1}{8s}+\frac{(\kappa-1)(\kappa-9)}{2!(8s)^2}+\ldots\right\} \qquad (\kappa = 4\eta^2)$$
$$\text{when } s\to\infty \text{ then } K_\eta(s) \approx \sqrt{\frac{\pi}{2s}}e^{-s} \tag{52}$$

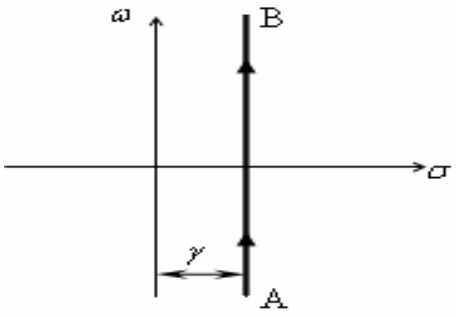

Figure 3 : Integration path

We break the integral into tow parts: one is a Dirac-deta function and the other is an integral with an integrant whose limit is zero when $s\to\infty$. Below, this procedure is performed as an example for computing $\sigma_{\theta\theta}$ in case 1, using the result of Eq.52

$$\int_{\gamma-i\infty}^{\gamma+i\infty}\frac{\Gamma_{\theta\theta}(r,\zeta)}{\Delta(s)}e^{s\zeta}ds = \int_{\gamma-i\infty}^{\gamma+i\infty}\left(\frac{\Gamma_{\theta\theta}(r,\zeta)}{\Delta(s)}-\lim_{|s|\to\infty}\frac{\Gamma_{\theta\theta}(r,\zeta)}{\Delta(s)}\right)e^{s\zeta}ds + \int_{\gamma-i\infty}^{\gamma+i\infty}\frac{M^2(3M^2-2)}{(3M^2-2)+4mm_s}\sqrt{\frac{a}{r}}\,e^{-ms\left(\frac{r}{a}-1\right)}e^{s\zeta}ds \tag{53}$$

And so

$$\frac{a\sigma_{\theta\theta}(r,\zeta)}{P_1} = \frac{1}{2\pi i}\int_{\gamma-i\infty}^{\gamma+i\infty}\left(\frac{\Gamma_{\theta\theta}(r,\zeta)}{\Delta(s)} - \frac{M^2(3M^2-2)}{(3M^2-2)+4mm_s}\sqrt{\frac{a}{r}}\,e^{-ms(\frac{r}{a}-1)}\right)e^{s\zeta}ds + \frac{M^2(3M^2-2)}{(3M^2-2)+4mm_s}\sqrt{\frac{a}{r}}\,\delta(\zeta - m(\frac{r}{a}-1)) \tag{54}$$

This simplifies to

$$\frac{a\sigma_{\theta\theta}(r,\zeta)}{P_1} = \frac{1}{2\pi}\int_{-\infty}^{+\infty} real\left(\left[\frac{\Gamma_{\theta\theta}(r,\zeta)}{\Delta(s)} - \frac{M^2(3M^2-2)}{(3M^2-2)+4mm_s}\sqrt{\frac{a}{r}}\,e^{-ms(\frac{r}{a}-1)}\right]e^{s\zeta}\right)d\omega + \frac{M^2(3M^2-2)}{(3M^2-2)+4mm_s}\sqrt{\frac{a}{r}}\,\delta(\zeta - m(\frac{r}{a}-1)) \tag{55}$$

The integral in the right side of Eq.55 should be calculated numerically. The numerical results apply for the following parameters:

$$M = \frac{V}{c_p} = 2$$
$$\upsilon = 0.25 \tag{56}$$
$$M_s = M\sqrt{\frac{2(1-\upsilon)}{1-2\upsilon}} = 3.4641$$

3.2 Numerical Integration

To find the inverse Laplace transform, the infinite integral should be calculated numerically. In this paper, adaptive Gauss/Lobatto integration method is used because of its more efficiency in comparison with adaptive Simpson method. The absolute error tolerance of integration and maximum function count are set to be 10^{-7} and 10^{6}, respectively. The time required to evaluate the response in 3040 points of the medium was nearly 60hours using MATLAB package, running on a Pentium VI-3.0GHz, 512Mb RAM. Consequently, it seems that it is impractical to calculate the solution for every point by numerical method.

4 Artificial Neural Network

*ANN*s are computational models which replicate the functions of a biological network composed of neurons. They are used to solve complex functions in various scientific applications such as process control, forecasting, optimization, classification, etc. An ANN can be trained to recognize patterns, therefore the nonlinear model developed during the training would allow ANN to generalize its conclusions and to be applicable to patterns not previously encountered [4], [5]. The *MLNN*s, which have features such as the ability to learn and generalize, smaller training set requirements, fast operation, ease of implementation and therefore most commonly used neural network architectures, have been adapted for estimating the response of the systems. As shown in Figure 4, a MLNN consists of (i) an input layer with neurons representing input variables to the problem, (ii) an output layer with neurons representing the dependent variables (what is being modeled), and (iii) one or more hidden layers containing neurons to help capture the nonlinearity in data.

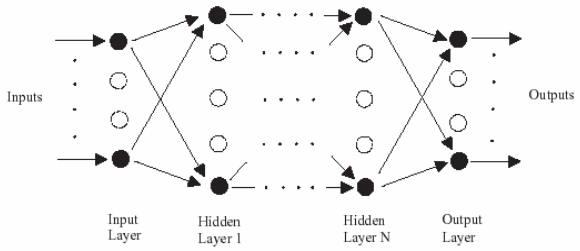

Figure 4 : Multilayer Neural Network Topology

4.1 Multilayer Neural Network (MLNN)

The most widely used ANN for engineering applications is known to be MLNN [9]. The MLNN is a nonparametric technique for performing a wide variety of detection and estimation tasks [4], [5], [7], [8], [10]. In the MLNN, each neuron j in the hidden layer sums its input signal x_i after multiplying them by the strengths of the respective connection weights w_{ji} and computes its output y_j as a function of the sum:

$$y_j = f\left(\sum w_{ji} x_i\right), \tag{57}$$

Where *f* is the activation function that is necessary to transform the weighted sum of all signals impinging onto a neuron. The activation function *(f)* can be a simple threshold function, or a sigmoidal, hyperbolic tangent, or radial basis function. The sum of squared differences between the desired and actual values of the output neurons *E* is defined as

$$E = \frac{1}{2}\sum_j \left(y_{dj} - y_j\right)^2 \tag{58}$$

Each weight w_{ji} is adjusted to reduce *E* as rapidly as possible. How w_{ji} is adjusted depends on the training algorithm adopted. Training algorithms are an integral part of ANN model development. A good training algorithm will shorten the training time, while achieving a better accuracy. There are a number of training algorithms used to train a *MLNN* and a frequently used one is called the backpropagation training algorithm. The backpropagation algorithm, which is based on searching an error surface using gradient descent for points with minimum error, is relatively easy to implement. However, backpropagation has some problems for many applications. It is not guaranteed to find the global minimum of the error function since gradient descent may get stuck in local minima, where it may remain indefinitely. Therefore, a lot of variations to improve the convergence of the backpropagation were proposed. Optimization methods such as second-order methods (conjugate gradient, quasi-Newton, Levenberg-Marquardt) have also been used for ANN training in recent years. The Levenberg-Marquardt algorithm combines the best features of the Gauss-Newton technique and the steepest-descent algorithm, but avoids many of their limitations. In particular, it generally does not suffer from the problem of slow convergence [11], [12]. Therefore, in this study the MLNN was trained with the Levenberg-Marquardt algorithm.

4.2 The Levenberg-Marquardt Algorithm

ANN training is usually formulated as a nonlinear least-square problem. Essentially, the *Levenberg-Marquardt* algorithm is a least-squares estimation algorithm based on the maximum neighborhood idea. Let $E(\mathbf{w})$ be an objective error function made up of m individual error terms $e_i^2(\mathbf{w})$ as follows:

$$E\left(\mathbf{w}\right) = \sum_{i=1}^{m} e_i^2\left(\mathbf{w}\right) = \left\| f\left(\mathbf{w}\right)\right\|^2 \tag{59}$$

where $e_i^2(\mathbf{w}) = \left(\mathbf{y}_{di} - \mathbf{y}_i\right)^2$ and $\mathbf{y}_{di}$ is the desired value of output neuron *i*, $\mathbf{y}_i$ is the actual output of that neuron. It is assumed that function $f(\cdot)$ and its Jacobian *J* are known at point **w**. The aim of the Levenberg-Marquardt algorithm is to compute the weight vector w such that $E(\mathbf{w})$ is minimum. Using the Levenberg-Marquardt algorithm, a new weight vector $\mathbf{w}_{k+1}$ can be obtained from the previous weight vector $\mathbf{w}_k$ as follows:

$$\mathbf{w}_{k+1} = \mathbf{w}_k + \delta\mathbf{w}_k \tag{60}$$

Where $\delta\mathbf{w}_k$ is defined as

$$\delta\mathbf{w}_k = -\left(J_k^T f\left(\mathbf{w}_k\right)\right)\left(J_k^T J_k + \lambda\mathbf{I}\right)^{-1} \tag{61}$$

4.3 Training

To find the stress and displacement components of the bore, the infinite integrals should be evaluated numerically as a function of $\frac{r}{a}$ and ζ. Because of the periodic nature of the integrand, the computational effort would be increased greatly to reach an acceptable accuracy. Consequently, MLNN can be used as a powerful tool to estimate the response of the plate. In order to train the ANN, the response in the set of 3040 points of the medium is used. Basic non-dimensional parameters, including $\frac{r}{a}$ and ζ, are used as the input layer while stress and displacement components are used as the output-layer components of the network. In the application, as mentioned above, the Levenberg-Marquardt algorithm has been used with two nonlinear hidden-layers. Tangent sigmoid (tansig) transfer function has been used and inputs and outputs are normalized within the range of (0, 1). The network structure is shown in Figure 5.

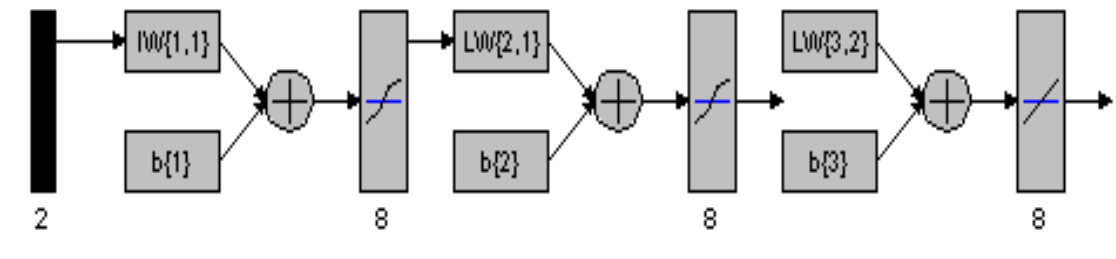

Figure 5 : Network structure

In the training stage, we used 8 neurons in both hidden layers by trial and error. 300 epochs of training carried out, as shown in figure 7, using 2700 patterns and successfully verified with the test data including 340 patterns as verification data which have not been used in the training. Using the results produced by network at the verification stage, the mean error percentage value was estimated to be 0.12%.

$$Mean\%Error = \frac{1}{p}\sum_{j=1}^{p}\left(100\frac{t_j - o_j}{t_j}\right) \tag{62}$$

The statistical results prove that the predictions provided by the network are close to the numerically evaluated results; therefore it can be used as an approximation to the response of the medium.

5 Results

The stress and displacement components contours for cases 1 and 2 are shown in figures 6 to 13. Also, the 3D plots of the radial (w) and longitudinal (u) displacements are shown in Figures 14 to 17.

It is obvious in the following figures that there is no stress or displacement ahead of the leading front. Furthermore, two formed mach cones because of the super seismic nature of the problem, that open toward the rear of the front in the medium, are detectable.

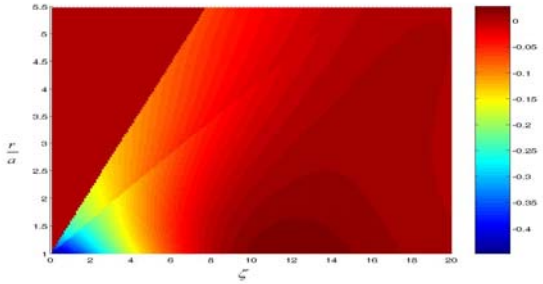

Figure 6 :The contour of the $\frac{a\sigma_{\theta\theta}}{P_1}$, case 1

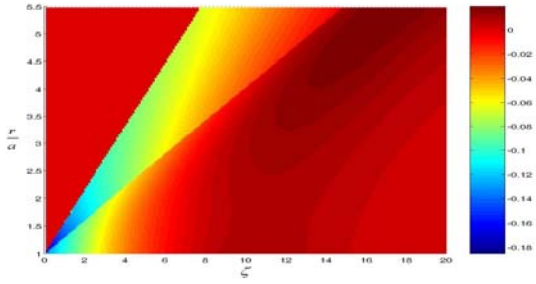

Figure 7 :The contour of the $\frac{a\sigma_{zz}}{P_1}$, case 1

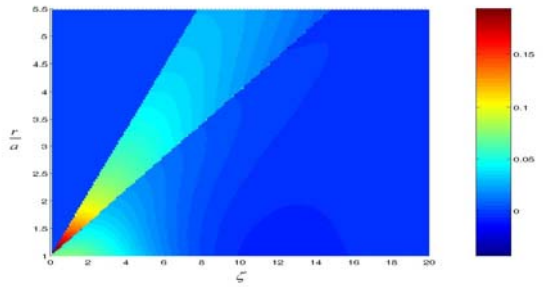

Figure 8 :The contour of the $\frac{a\sigma_{\theta\theta}}{P_2}$, case2

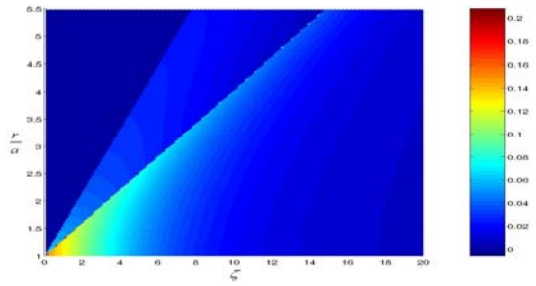

Figure 9 :The contour of the $\frac{a\sigma_{zz}}{P_2}$, case 2

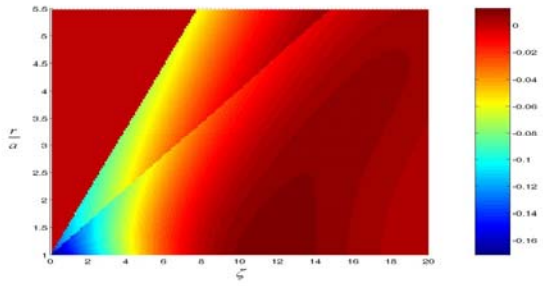

Figure 10 :The contour of the $\frac{\mu w}{P_1}$, case 1

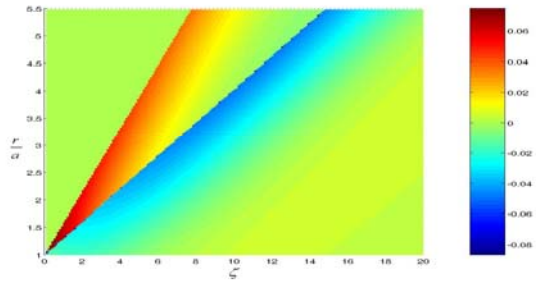

Figure 11 :The contour of the $\frac{\mu u}{P_1}$, case1

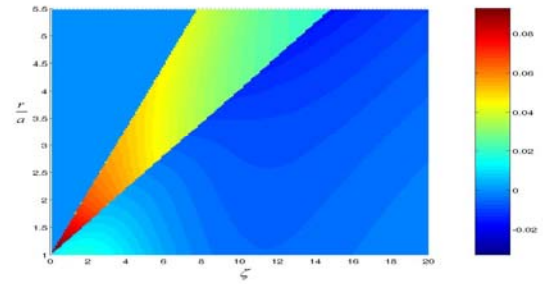

Figure 12 :The contour of the $\frac{\mu w}{P_2}$, case2

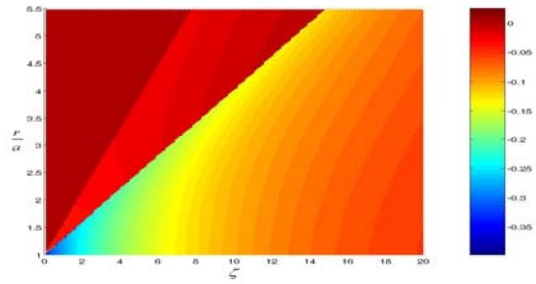

Figure 13 :The contour of the $\frac{\mu u}{P_2}$, case2

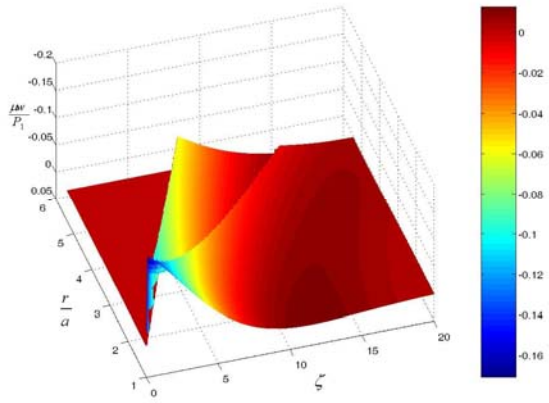

Figure 14 :The 3D plot of the $\frac{\mu w}{P_1}$, case 1

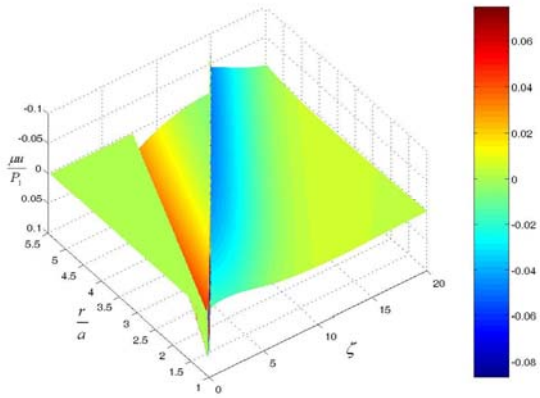

Figure 15 :The 3D plot of the $\frac{\mu u}{P_1}$, case1

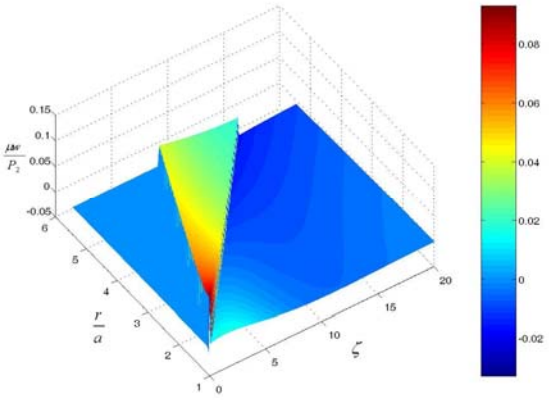

Figure 16 :The 3D plot of the $\frac{\mu w}{P_2}$, case2

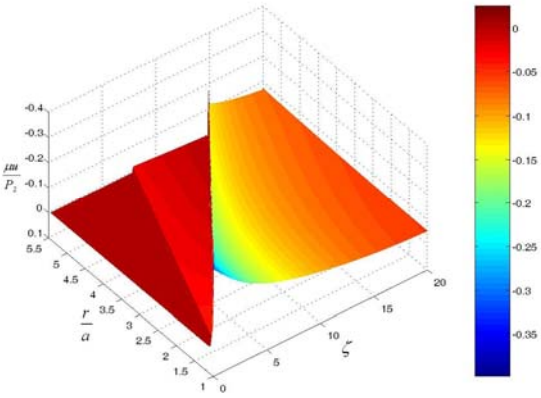

Figure 17 :The 3D plot of the $\frac{\mu u}{P_2}$, case2

6 Conclusion

The feedforward backpropagation neural network, consists of two nonlinear hidden layers, successfully estimated the response of the medium subjected to moving load. It was trained by the response of the medium in a finite set of points using Levenberg-Marquardt backpropagation method. The computational effort decreased considerably in comparison with numerical methods which are extremely time-consuming.

It shows that soft computing method such as neural network can be used as powerful tools in estimating the response of the infinite medium and spatial structures subjected to moving loads.

References

[1] M. Aliakbarian, J. Johnson. Oblique incidence of plane stress waves on a thick cylindrical shell, *Air force weapon laboratory*, 1969.

[2] R. Parnes, M. Baron, Moving loads on the surface of a cylindrical bore, *United air force project RAND*, 1965.

[3] S. Paul, M. Aliakbarian, J. Johnson. Interaction of plane elastic waves with a thick cylindrical shell, *Air force weapon laboratory*, 1965.

[4] A. Hajati, M. Movassat, M. ShariatPanahi, A neural-net based matching procedure for turbocharged SI-engines, *Proceeding of applied thermodynamics*, Istanbul, Turkey, 2005.

[5] M. Nikkhah-Bahrami, A. Hajati, Response of an elastic plate to moving load using neural network, Proceeding of ASME/SES/ASCE joint conf. McMAT2005, Louisiana, 2005.

[6] P. Morse, H. Feshbach, *Methods of theoretical physics*, 1994.

[7] Haykin, S., *Neural Networks: A Comprehensive Foundation*, Macmillan, New York, 1994.

[8] Basheer I.A., Hajmeer M., Artificial neural networks: fundamentals, computing, design, and application, *J. Microbiol. Meth.*, **43**: 3–31., 2000.

[9] Guler, N., Ubeyli, E., Wavelet-based neural network analysis of ophthalmic artery Doppler signals, *J. computers in biology and medicine*, 2004.

[10] Chaudhuri B., Bhattacharya U., Efficient training and improved performance of multilayer perceptron in pattern classification, *Neurocomputing*, **34**: 11–27, 2000.

[11] Hagan M., Menhaj M., Training feedforward networks with the Marquardt algorithm, *IEEE Trans. Neural Networks*, **6**: 989–993, 1994.

[12] Battiti R., First- and second-order methods for learning: between steepest descent and Newton's method, *Neural Comput.* **4**: 141–166, 1992.

[13] Abramowitz, M., 1964, Handbook of mathematical functions, pp. 378.